ACS APPLIED MATERIALS & INTERFACES

Research Article

www.acsami.org

One-Step Process for Superhydrophobic Metallic Surfaces by Wire Electrical Discharge Machining

Won Gyu Bae,[†,‡] Ki Young Song,[‡] Yudi Rahmawan,[‡,§] Chong Nam Chu,[‡] Dookon Kim,[‡] Do Kwan Chung,*[,‡,∥] and Kahp Y. Suh*[,†,‡]

[†]Interdisciplinary Program of Bioengineering and [‡]School of Mechanical and Aerospace Engineering, Seoul National University, Seoul 151-742, Korea

[§]Department of Materials Science and Engineering, University of Pennsylvania, Philadelphia 19104, United States

[∥]School of Robot and Automation Engineering, Dongyang Mirae University, Seoul 152-714, Korea

Supporting Information

ABSTRACT: We present a direct one-step method to fabricate dual-scale superhydrophobic metallic surfaces using wire electrical discharge machining (WEDM). A dual-scale structure was spontaneously formed by the nature of exfoliation characteristic of Al 7075 alloy surface during WEDM process. A primary microscale sinusoidal pattern was formed via a programmed WEDM process, with the wavelength in the range of 200 to 500 μm. Notably, a secondary roughness in the form of microcraters (average roughness, Ra: 4.16 to 0.41 μm) was generated during the exfoliation process without additional chemical treatment. The low surface energy of Al 7075 alloy (γ = 30.65 mJ/m^2) together with the presence of dual-scale structures appears to contribute to the observed superhydrophobicity with a static contact angle of 156° and a hysteresis less than 3°. To explain the wetting characteristics on dual-scale structures, we used a simple theoretical model. It was found that Cassie state is likely to present on the secondary roughness in all fabricated surfaces. On the other hand, either Wenzel or Cassie state can present on the primary roughness depending on the characteristic length of sinusoidal pattern. In an optimal condition of the serial cutting steps with applied powers of ~30 and ~8 kW, respectively, a stable, superhydrophobic metallic surface was created with a sinusoidal pattern of 500 μm wavelength.

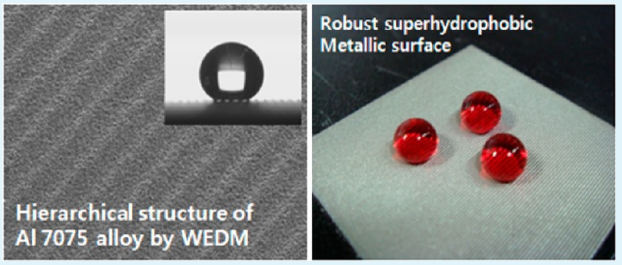

KEYWORDS: *superhydrophobicity, metallic surface, dual-scale roughness, microcraters, wire electrical discharge machining*

INTRODUCTION

The unique wetting properties of lotus leaves have been a fascinating subject of research for many decades because of the fundamental interests in wetting and directional flow of water.[1,2] Lotus effect provides a variety of advantages such as non-wetting, self-cleaning from any dirts, and small flow resistance.[3] Extensive studies have been carried out to understand the mechanism of water repellency and self-cleaning behavior of lotus leaves.[4−9] It is now widely accepted that superhydrophobicity is orchestrated by the existence of micro- and nanostructures on the low energy surface. Also, the scientists revealed that a distinctive hierarchical structure on the lotus leaves plays a key role in maintaining water repellency and self-cleaning behaviors.[10,11]

A great number of methods have been developed to achieve artificial superhydrophobic surfaces.[12,13] Examples include self-assembly of nanoparticles,[14,15] lithographic patterning,[16,17] sol−gel method,[18] chemical vapor deposition,[19] electrospinning,[20] templating,[21] and plasma fluorination.[22] Despite the success of previous methods for extremely high contact angle (CA) (> 150°) and low CA hysteresis (< 5°), the surfaces have been usually made of soft materials such as polymers or colloidal materials. Furthermore, the methods often required an additional hydrophobic treatment on the intrinsically hydrophilic surfaces. Superhydrophobic surfaces made of soft materials may be fragile when exposed to mechanical impact such as raindrops or scratching. Moreover, the stability of hydrophobic coating is largely limited by an aging process.[23] Therefore, it is potentially of great benefit to develop a method to make a robust metallic superhydrophobic surface that does not collapse or deteriorate over time, which would facilitate the widespread use of superhydrophobic surfaces in industrial applications.

Many attempts have been made to achieve robust superhydrophobic surfaces over mechanical wears and chemical deterioration using metallic surfaces, which offer higher durability and robustness under harsh applications such as aerospace engines, ship hulls, and automobiles. To create roughness on metallic surfaces, diverse methods have been proposed, such as laser texturing-chemical etching,[24] one-step

Received: May 4, 2012
Accepted: June 26, 2012
Published: June 26, 2012

   dx.doi.org/10.1021/am3007802 | ACS Appl. Mater. Interfaces 2012, 4, 3685−3691

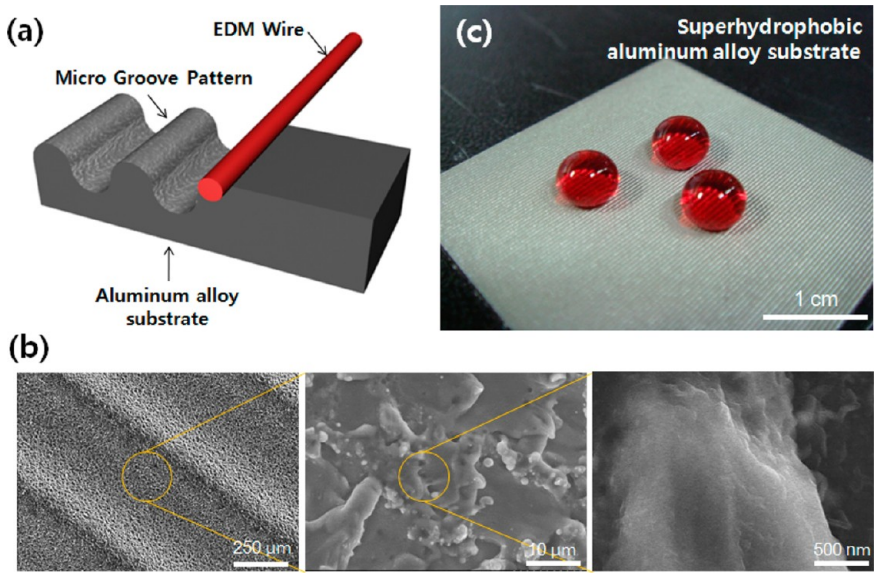

Figure 1. (a) Schematic illustration to fabricate dual-scale structures on the Al alloy surface by WEDM. By using a single step machining of sinusoidal patterns, a secondary roughness is spontaneously formed due to surface exfoliation process. (b) SEM images of a machined Al surface with distinct dual-scale structures. Magnified views are also shown. (b) Optical image of droplets of dyed-DI water on the fabricated Al surface.

femtosecond laser irradiation,[25,26] sandblasting,[27] solution-immersion process,[28] anodic oxidation,[29,30] chemical etching,[31,32] electrochemical etching,[33] boiling water immersion,[34] and coating method.[35] In the laser texturing-chemical etching, a steel surface is structured with a microscale roughness by using various laser power densities and texture directions. However, the method has potential weaknesses such as requirement of two-step processes (laser texturing and chemical etching) and use of flat two-dimensional surfaces to make a hierarchical structure. Laser irradiation is a more improved way to texture a metallic surface, yet it still requires pretreatment such as chemical coating or polishing. Therefore, the methods based on laser would not be suitable for generating hierarchical structures on curvature surfaces. In the sandblast and solution-immersion processes, a superhydrophobic metallic surface can be easily generated but a two-step fabrication process is still needed in the form of etching and chemical coating. Furthermore, it is hard to make well-defined dual-roughness surfaces with minimum run-to-run variations. Until now, it has not been demonstrated to build a superhydrophobic metallic surface with a finely controlled hierarchical surface morphology in a minimal one-step process, which does not involve an additional pretreatment step such as polishing and chemical treatment.

In this work, we present a one-step process for fabricating superhydrophobic metallic surface with hierarchical architecture by using wire electrical discharge machining (WEDM) and intrinsically hydrophobic Al 7075 alloy. Al alloys have been used in many industrial applications due to their superb properties, such as high corrosion resistance, good mechanical properties, abundance, and low weights. In addition to these properties, the Al 7075 alloy used in our experiment has a low surface energy (γ = 30.65 mJ/m^2). In general, electrical discharge machining (EDM) utilizes a high potential difference between electrode and workpiece materials under a dielectric liquid. The shapes of workpiece materials can be controlled by the movement of electrode when a high potential difference melts or vaporizes workpiece materials. There are several types of EDM processes: die-sinking EDM, microEDM, and WEDM.[36,37] In our work, WEDM is employed because it uses a wire as an electrode to cut workpiece materials with features that can accommodate formation of complicated structures using a programmed wire path. During a EDM process, an electrode and a workpiece are immersed in a dielectric fluid such as kerosene and de-ionized (DI) water.[38,39] Generally, the working fluid for EDM has high resistivity, which keeps dielectric strength as the voltage is applied to an electrode and a workpiece. When the electrode approaches the surface of workpiece materials in a relatively narrow distance, the working fluid loses the dielectric character and becomes the medium of discharge sparks. Subsequently, when a high voltage is provided within the gap, an electrical discharge is initiated, in which electrical energy is converted into heat. As a result, a small amount of material is melted and vaporized at the electrode and workpiece.[39,40] In this process, a small cavity, called crater, is generated both on the electrode and workpiece surfaces, ultimately leading to the formation of randomly distributed craters. These craters are potentially useful to create roughness in different length scales for superhydrophobicity.

The surface roughness of these craters is determined by various discharge conditions such as discharge current and duration. In this sense, WEDM seems useful because of its ability to generate roughness on metallic surfaces simply by controlling electric pulse parameters.[41] Additionally, there are several potential advantages of WEDM. First, a microscale sinusoidal pattern can be formed by a simple programming of wire path with a wide range of wavelengths (λ = 200−500 μm).[36] Second, it is possible to texture a curved surface with careful consideration for the profile of the workpiece. Third, a secondary microscale roughness is spontaneously created on the machined surface in the form of craters. Taken together, the nature of WEDM process will provide a hierarchical structure in one-step process without additional chemical treatment, which leads to a robust, superhydrophobic surface suitable for many industrial applications.

EXPERIMENTAL SECTION

Materials. We used a commercially available Al 7075 alloy (duralumin). The Al 7075 alloy is composed of Al (87.1−91.4%),

Table 1. Cross-Sectional Profiles of the Primary Roughness Formed on the Surface of Al 7075 Alloy by WEDM

Wavelength, λ [μm]	Profile	Amplitude [μm]	Aspect ratio	Roughness factor
500		74	1.44	1.059
400		46	1.33	1.043
300		25	1.23	1.016
200		10	1.13	1.003

Cr (0.18−0.280%), Cu (1.20−2.0%), Fe (<0.50%), Mg (2.10−2.90%), Mn (< 0.30%), Si (<0.40%), Ti (<0.20 %), and Zn (5.10−6.10%). This alloy is widely used in the structural components of aircraft and automotive industries because of its exceptionally high strength to weight ratio.[42]

Contact Angle Measurements. Static contact angles (CAs) and CA hysteresis of liquids used in experiment were measured using DSA100 goniometer (Kruss, Germany). In each measurement, 6 μL of liquid was dispensed on the surface over the time span of 1.5 min. The measurement was averaged over at least six different locations for each sample conditions.

Surface Energy Measurement. The surface energy was evaluated using the Owens-Wendt method with deionized (DI) water and formamide (de-ionized, 99.5%, Sigma) as two probing liquids.[43] The wetting angles of both liquids were measured on nearly idealized-flat Al 7075 alloy surface. To achieve idealized flat- Al 7075 alloy surface, the bulk sample was ground with multi-step sand paper grinding of different grits from 320, 600, 1000, and 1500 accompanied by water flowing as lubricant. Finally, the sample was polished with alumina powder suspension.[44] A shiny flat Al 7075 alloy was achieved after the process to simulate the idealized-flat surface for wetting angle measurement.

Scanning Electron Microscopy. SEM images were obtained using SEM (S-4800, Hitachi, Japan) at an acceleration voltage of 15.0 kV and an average working distance of 11.4 mm.

White Light Scanning Interferometry. To acquire average roughness and morphologic images of the dual-scale roughness metallic surfaces, we mounted the specimen on a stage of non-contact three-dimensional surface profiler (NanoView-E1000; NanoSystem, Daejeon, Korea). Images of 600 μm × 500 μm area were acquired accordingly.

RESULTS AND DISCUSSION

Figure 1a illustrates a schematic of the WEDM process for fabricating dual-scale roughness on metallic surfaces with superhydrophobicity. Here, the primary roughness is formed in the shape of sinusoidal profile in several hundreds of micrometer wavelength (see Table 1) and the secondary roughness is naturally generated with crater-like structures of a few micrometers (Figure 1b), covering the entire Al 7075 alloy surface. As seen from Figure 1c, the fabricated surface shows visible microscale wavy patterns (λ = 500 μm) with superhydrophobicity (CA > 156 ± 5°). To demonstrate the water-repellency on the as-prepared metallic surface, we recorded the free falling of water drops with a high-speed camera (Redlake HS4-C-2) at a rate of 500 frames/s with the pixel resolution of 436 × 416 (see Figure S1 in the Supporting Information).

In this research, a commercial WEDM machine (EZ20S, Seoul Precision Machine Co., Ltd.) was used to make sinusoidal patterns and surface roughness, and DI water was used as the dielectric fluid in the machining process. Because both the electrode and workpiece are machined simultaneously in the EDM process, a wire feed system needs to continuously supply a wire electrode for machining accuracy and prevent the wire breakage as shown in Figure 2a. The substrate used in this study was an Al 7075 alloy with the dimension of 30 mm length × 30 mm width × 2 mm thickness.

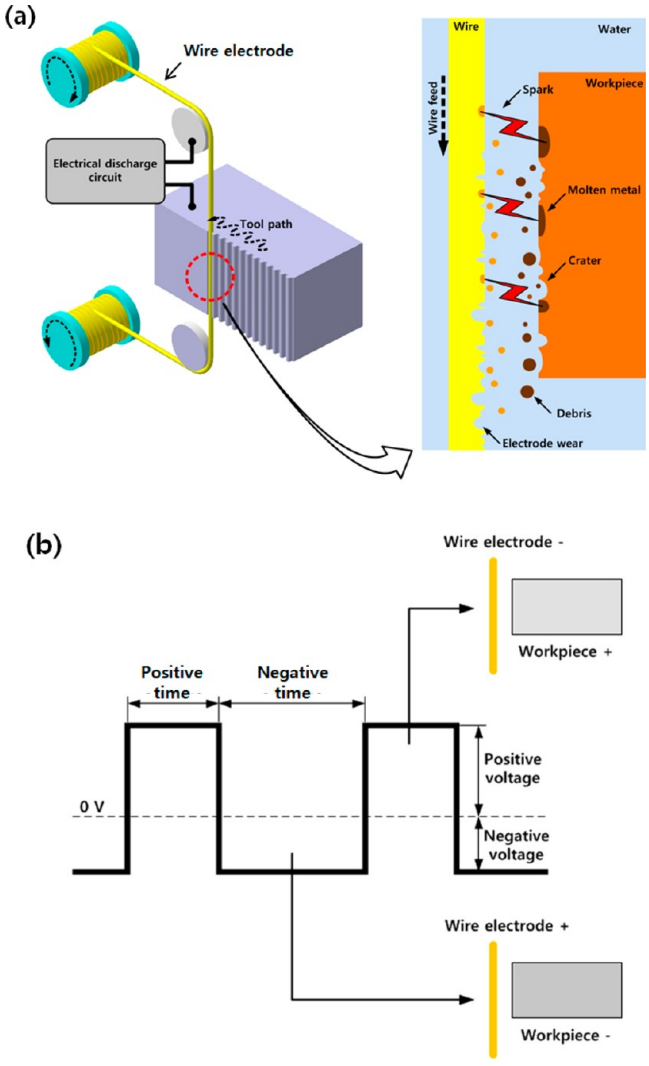

Figure 2. (a) Schematic diagram of WEDM process. (b) A waveform of voltage between a workpiece and a wire electrode.

In Figure 2b, a square wave AC voltage was applied to the machining gap between the wire electrode and the workpiece for anti-corrosion.[45] Here, the positive duration ranged from 15 to 30 μs, and the negative duration from 20 to 50 μs (see Table S1 in the Supporting Information). It is interesting to note that the average roughness was increased almost linearly with the increase of the applied energy in the WEDM process (i.e., applied voltage and current) and the charging duration. It seems that the formation of craters is attributed to the localized melting and evaporation of the surface due to the applied

dx.doi.org/10.1021/am3007802 | ACS Appl. Mater. Interfaces 2012, 4, 3685−3691

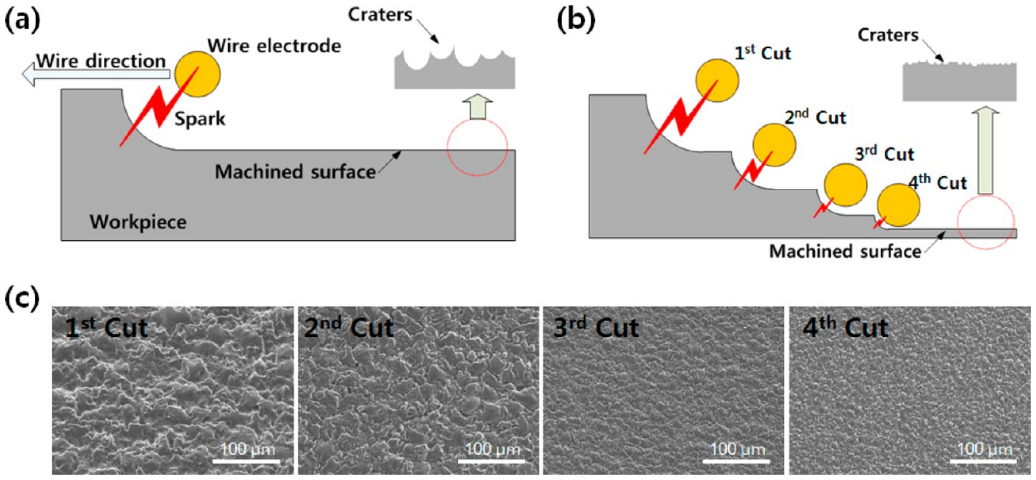

Figure 3. Schematic of the fabrication process with different machining conditions to obtain (a) rough and (b) smooth surfaces. (c) SEM images of the secondary roughness with various cutting conditions.

charges. The local defects and/or weak phases on Al 7075 alloy surface may become the initial seed for craters formation when a high potential energy difference is applied. In this case, the application of a higher energy will result in a highly localized increase of temperature for melting and evaporation of workpiece. Therefore, a larger crater or roughness can be made using a higher applied energy as shown in Table S1 in the Supporting Information.

In the conventional WEDM process, a four-step process involving different applied energy has been implemented for smooth machining. In our experiment, the largest electrical discharge energy was applied in the first cutting, resulting in the highest surface average roughness of 4.16 μm (Figure 3a). The purpose of the first cut was to create a deep cutting profile in accordance with the programmed shape. In the subsequent cutting steps, the applied energy was gradually reduced in such a way that the surface average roughness monotonically decreased from 2.35 to 0.41 μm (Figure 3b). Therefore, the surface became highly smooth and polished after the four cutting steps. Figure 3c shows the SEM images of WEDM processed Al 7075 alloy surface with secondary roughness from 1st to 4th cut.

To perform a detailed study on the effect of WEDM process parameters such as roughness and wetting angles, we classified the samples on the basis of the number of cutting steps and sinusoidal wavelength. As shown in Table 2, 16 different types of surfaces were fabricated by the WEDM and subsequently analyzed with CA measurements. For convenience, the samples were divided into four groups (4 samples in each group) depending on the wavelength of sinusoidal patterns: 200, 300, 400, and 500 μm. All samples in each group were subjected to a series of four cutting steps following the conditions in Table S1 in the Supporting Information.

Table 2. Set of Samples with Different Types of Surfaces Profiles and Their CAs

	CA (deg)			
	λ = 200 μm	λ = 300 μm	λ = 400 μm	λ = 500 μm
1st cut	141.9	142.5	154.3	156.5
2nd cut	139.0	139.4	151.1	154.8
3rd cut	136.5	137.2	138.9	140.3
4th cut	134.3	136.0	136.2	140.8

Figure 4a shows a series of three-dimensional morphology images of the secondary roughness formed from the WEDM cutting process. The first cut of WEDM process with the highest energy produced the highest average roughness (Ra ~4.16 μm) because of the formation of large craters. The second, third and fourth cuts, with lower energies, produced lower average roughness of 2.37, 0.94, 0.41 μm, respectively, suggesting that there is a linear correlation between the surface roughness and the applied energy. The measured water CAs on the fabricated surfaces are shown in Figure 4b along with comparisons to the theoretical models. Here, we employed the recent theoretical models by integrating the Wenzel and Cassie states on dual-scale structures, in which the wetting states can be categorized into four types:[5]

Wenzel–Wenzel or W'-W'':

$$\cos\theta_{app}^{W'-W''} = R'R''\cos\theta_e \quad (1)$$

Wenzel–Cassie or W′-C″:

$$\cos\theta_{app}^{W'-C''} = R'\{f''(\cos\theta_e + 1) - 1\} \quad (2)$$

Cassie–Wenzel or C′-W″:

$$\cos\theta_{app}^{C'-W''} = R''\{f'(\cos\theta_e + 1) - 1\} \quad (3)$$

Cassie–Cassie or C′-C″:

$$\cos\theta_{app}^{C'-C''} = f'f''(\cos\theta_e + 1) - 1 \quad (4)$$

where R, f, θ_e represent the roughness, solid fraction, and equilibrium wetting angle, respectively, and the single and double apostrophes represent the first and second hierarchy scales, respectively. On the basis of the calculation of wetting angles on the secondary roughness of Al 7075 alloy, all cutting stages of WEDM produced the surfaces in the Cassie regime (C″ state) with relatively low CA hysteresis (CAH) of 8.2, 10.7, 13.2, and 15.8°, respectively (in the order of 1st to 4th cut). The Wenzel model for the same roughness values turned out to deviate largely from the experimental observations. In contrast, the Cassie–Baxter model yielded highly matched CAs with the estimated air fractions of the secondary roughness ($1 - f''$) in the range from 0.65 to 0.5 with its respective surface from 1st to 4th cut. It is indicative that the wetting state in the secondary

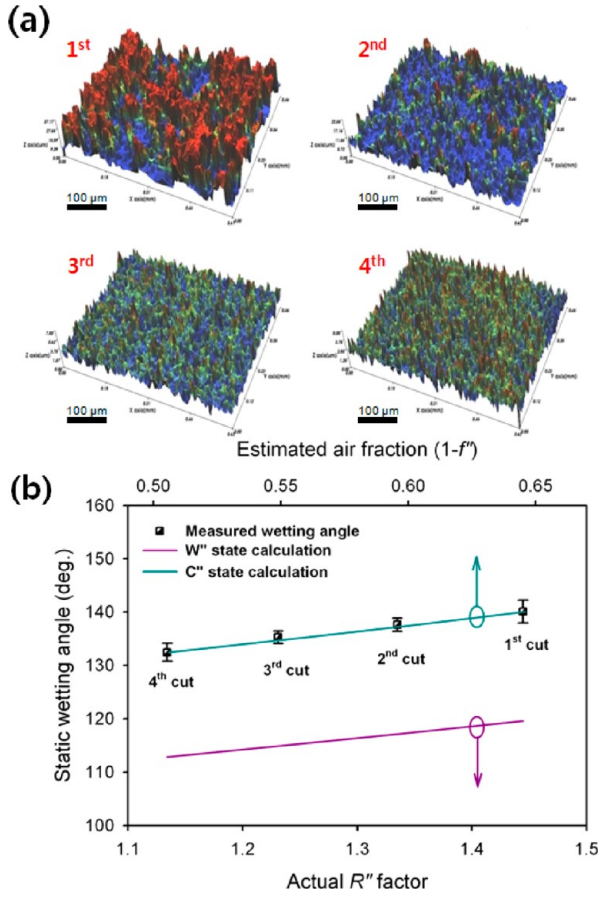

Figure 4. (a) Three-dimensional images of metallic surfaces after WEDM process taken by surface profiler. As shown, the 1st cut with higher energy produces the roughest surface compared to those in the 2nd, 3rd, and 4th cuts with lower energies. The static wetting angles on the corresponding surfaces are shown in (b) with comparisons with the theoretical models using the Wenzel (purple line) and Cassie (blue line) states. Note that experimental measurements are highly matched with the Cassie state in all surfaces.

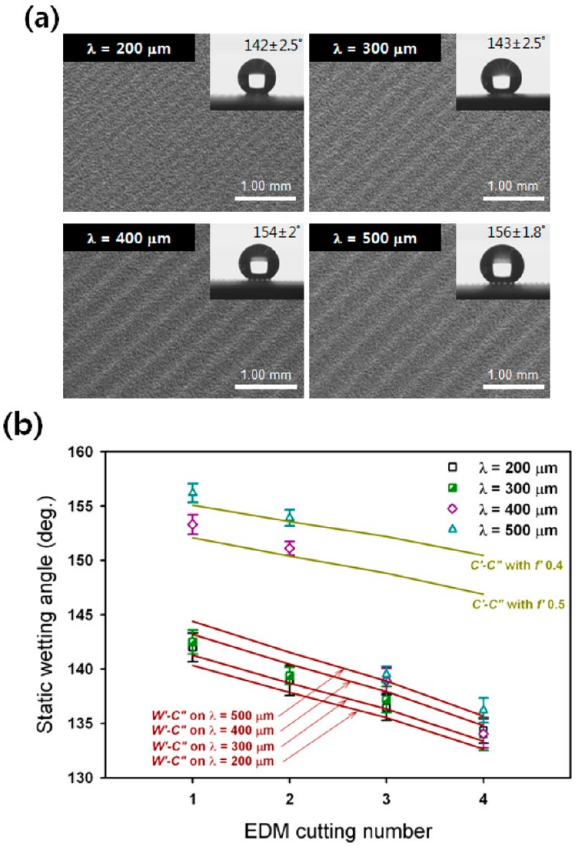

Figure 5. (a) SEM images of hierarchical structures on metallic surfaces with various wavelengths (λ) of sinusoidal micropatterns. The optical images of water droplets are shown in the inset. (b) Static wetting angles on the various samples in (a) with comparisons to the theoretical models. As shown, the wetting states are highly matched with the C′-C″ state (superhydrophobic) for the samples with λ = 400 and 500 μm with the 1st and 2nd cuts. For the 3rd cut or higher, a transition to the W′-C″ state is observed. For the samples with λ = 200 and 300 μm, the W′-C″ state is likely to exist in all surfaces.

roughness is stable in the Cassie–Baxter state. Therefore, we conclude that the possible wetting states in dual-scale roughness are only W′-C″ and C′-C″ in eqs 2 and 4.

Further measurements of wetting angles after the 1st cut are shown in Figure 5a. Here, the microscale sinusoidal patterns with different wavelength show different wetting behaviors. For higher wavelengths (500 and 400 μm) with the 1st and 2nd cuts, the CAs were larger than 150° with CAH being lower than 3°. In contrast, for lower wavelengths (200 and 300 μm) with all cuts and higher wavelengths with the 3rd and 4th cuts, CAs were ~140° with higher CAH (> 5°). For the 1st and 2nd cuts in the wavelength of 500 and 400 μm, there was no significant difference in CAs when viewed from the front (0°) and the side (90°) because the surfaces were in the C′-C′ state. However, there was a slight difference in CAs (<5°) when viewed from the both directions when the surface was in the W′-C′ state (see Figure S2 in the Supporting Information). Detailed comparisons of the CAs (Table 2) with the theoretical models are shown in Figure 5b. Here, for higher wavelengths with the 1st and 2nd cuts, the experimental data show good agreement with the C′-C″ state. Then, there seems a transition to W′-C″ state with the 3rd and 4th cuts. We postulate that the transition from the C′-C″ to W′-C″ is mainly due to a decrease of the amplitude of the surface's sinusoidal profile as provided in Table 1. In parallel, for lower wavelengths the experimental measurements show excellent agreement with the W′-C″ state. This suggests that the WEDM method presented here has designing capability to tune surface texture and wettability.

To verify the potential for an industrial use of a superhydrophobic Al alloy presented here, we prepared two contrasting samples as demonstrated in Figure 6: a metallic surface and a replicated polymer surface made with perfluoropolyether (PFPE) via UV-assisted capillary force lithography.[47] After scratching both samples in a controlled manner with a P3000 sandpaper (mean particle diameter: 7 μm, sandblasting with 1.0 mm/s at a stroke of 10 cm), the surface morphologies and wetting properties were examined. When the preload was increased up to 2 N/cm^2, the metallic surface was found to remain intact, preserving the initial superhydrophobicity. In sharp contrast, the polymer surface lost its water-repellency because of the mechanical damage on the surface. On the basis of this observation, the Al alloy surface would be appropriate for industrial uses with harsh environments.

dx.doi.org/10.1021/am3007802 | ACS Appl. Mater. Interfaces 2012, 4, 3685–3691

Table 3. Surface Energy Measurement of Al 7075 Alloy Used in Our Experiment

θ_e^{water} (deg.)	$\theta_e^{formimide}$ (deg.)	γ^{polar} (mJ/m^2)	$\gamma^{dispersive}$ (mJ/m^2)	γ (mJ/m^2)
109.5 ± 1.29	81.12 ± 0.85	0.07 ± 0.04	30.58 ± 1.38	30.65 ± 1.42

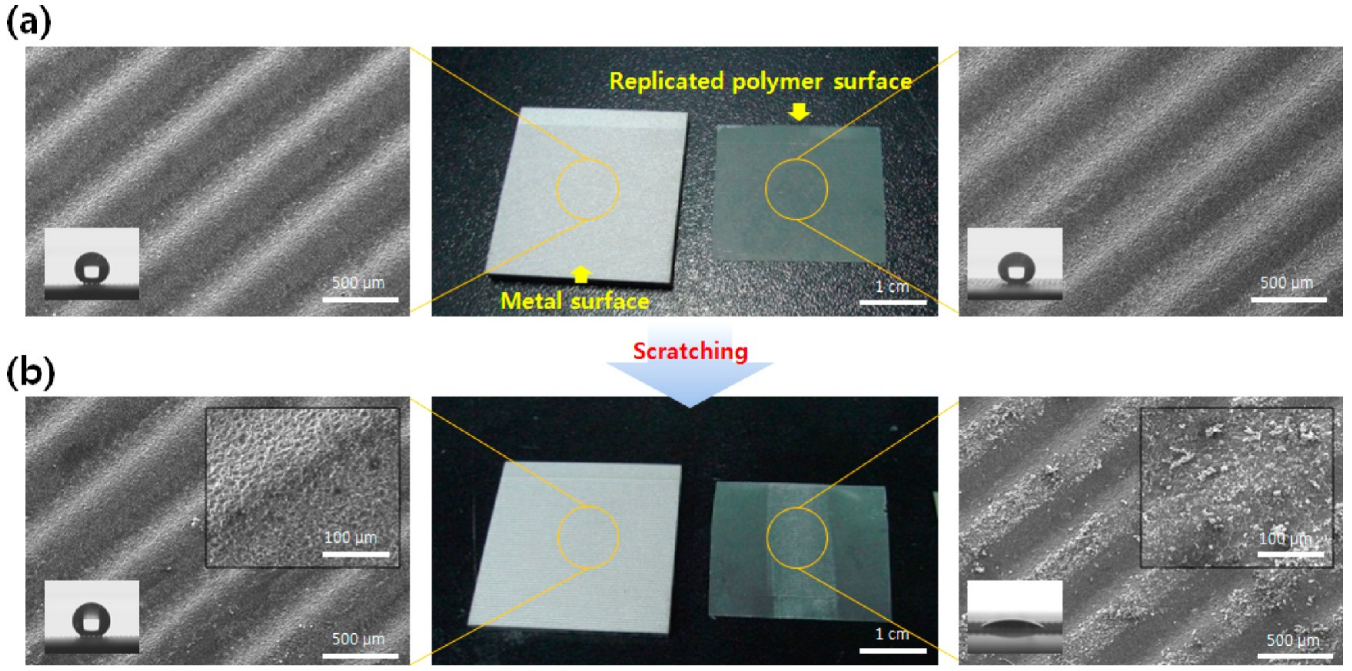

Figure 6. Verification of the mechanical robustness with scratch tests using superhydrophobic Al alloy and its replicated perfluoropolyether (PFPE) surfaces. (a) Optical and SEM images of the as-prepared Al and polymer surfaces. As shown, the initial morphologies are nearly the same. Each inset shows the measured CA of 156 and 165°, respectively. (b) Optical and SEM images of the samples after scratching tests using a P3000 sand paper. As shown, the Al alloy surface remained intact, whereas the polymer surface was damaged with many debris and scratches. Each inset shows the corresponding CA as well as a magnified view of the surface. For the polymer surface, the CA dropped to ~15°.

CONCLUSIONS

We have presented a direct, one-step method to form dual-roughness superhydrophobic metallic surfaces by using WEDM process. Unlike the conventional methods involving a two-step fabrication of etching and coating, the current method allows for a robust metallic surface with the help of a one-step process involving a programmed wire path. A secondary roughness of several micrometers was spontaneously generated because of the exfoliation process without additional chemical treatment. The wetting state analysis demonstrated the presence of the Cassie state in the secondary roughness regardless of the machining conditions. Therefore, on dual-scale structures of metallic surfaces after the WEDM process, the corresponding wetting states were identified to be either the C′-C″ state with a higher wavelength in the 1st and 2nd cuts or the W′-C″ state in the 3rd and 4th cuts with a lower wavelength. This finding will be useful in designing an optimum process of superhydrophobic metallic surfaces by WEDM. It is further envisioned that the WEDM method presented here will find many uses in preparing superhydrophobic metallic surfaces in more diverse applications with harsh environments.

ASSOCIATED CONTENT

Supporting Information

Snapshots of high-speed camera images, optical images of droplets in two directions, images of the custom-built equipment and WEDM process conditions. This material is available free of charge via the Internet at http://pubs.acs.org.

AUTHOR INFORMATION

Corresponding Author

* Tel +82-2-2610-5186 (D.K.C.); +82-2-880-9103(K.Y.S.). Fax +82-2-2610-1852 (D.K.C.); +82-2-883-1597 (K.Y.S.). E-mail: dkchung@dongyang.ac.kr (D.K.C.); sky4u@snu.ac.kr (K.Y.S.).

Notes

The authors declare no competing financial interest.

ACKNOWLEDGMENTS

We gratefully acknowledge support from National Research Foundation of Korea (NRF) grant (2011-0017530 and 2011-001572), WCU (World Class University) program (R31-2008-000-10083-0) and Basic Science Research Program (2010-0027955). This work was also supported in part by Korea Research Foundation Grant (KRF-J03003) and the Global Frontier R&D Program on Center for Multiscale Energy System.

REFERENCES

(1) Zheng, Y.; Bai, H.; Huang, Z.; Tian, X.; Nie, F. Q.; Zhao, Y.; Zhai, J.; Jiang, L. *Nature* **2010**, *463*, 640−643.
(2) Sun, T.; Feng, L.; Gao, X.; Jiang, L. *Acc. Chem. Res.* **2005**, *38*, 644−652.
(3) Zhang, X.; Shi, F.; Niu, J.; Jiang, Y.; Wang, Z. *J. Mater. Chem.* **2008**, *18*, 621−633.
(4) Lafuma, A.; Quéré, D. *Nat. Mater.* **2003**, *2*, 457−460.
(5) Rahmawan, Y.; Moon, M. W.; Kim, K. S.; Lee, K. R.; Suh, K. Y. *Langmuir* **2009**, *26*, 484−491.
(6) Cassie, A.; Baxter, S. *Trans. Faraday Soc.* **1944**, *40*, 546−551.

(7) Wenzel, R. N. *Ind. Eng. Chem* **1936**, *28*, 988−994.
(8) Shibuichi, S.; Onda, T.; Satoh, N.; Tsujii, K. *J. Phys. Chem.* **1996**, *100*, 19512−19517.
(9) Gao, L.; McCarthy, T. J. *Langmuir* **2009**, *25*, 14105−14115.
(10) Gao, L.; McCarthy, T. J. *Langmuir* **2006**, *22*, 2966−2967.
(11) Cha, T. G.; Yi, J. W.; Moon, M. W.; Lee, K. R.; Kim, H. Y. *Langmuir* **2010**, *26*, 8319−8326.
(12) Li, X. M.; Reinhoudt, D.; Crego-Calama, M. *Chem. Soc. Rev.* **2007**, *36*, 1350−1368.
(13) Liu, K.; Yao, X.; Jiang, L. *Chem. Soc. Rev.* **2010**, *39*, 3240−3255.
(14) Xu, L.; Karunakaran, R. G.; Guo, J.; Yang, S. *ACS Appl. Mater. Interfaces* **2012**, *4*, 1118−1125.
(15) Du, X.; Li, X.; He, J. *ACS Appl. Mater. Interfaces* **2010**, *2*, 2365−2372.
(16) Shiu, J. Y.; Kuo, C. W.; Chen, P.; Mou, C. Y. *Chem. Mater.* **2004**, *16*, 561−564.
(17) Jeong, H. E.; Kwak, M. K.; Park, C. I.; Suh, K. Y. *J. Colloid Interf. Sci.* **2009**, *339*, 202−207.
(18) Zheng, Y.; Jiang, L.; Wang, J.; Han, D. *Appl. Phys. Lett.* **2008**, *93*, 094107.
(19) Tavana, H.; Amirfazli, A.; Neumann, A. *Langmuir* **2006**, *22*, 5556−5559.
(20) Lim, H. S.; Baek, J. H.; Park, K.; Shin, H. S.; Kim, J.; Cho, J. H. *Adv. Mater.* **2010**, *22*, 2138−2141.
(21) Guo, C.; Feng, L.; Zhai, J.; Wang, G.; Song, Y.; Jiang, L.; Zhu, D. *ChemPhysChem* **2004**, *5*, 750−753.
(22) Woodward, I.; Schofield, W.; Roucoules, V.; Badyal, J. *Langmuir* **2003**, *19*, 3432−3438.
(23) Morra, M.; Occhiello, E.; Marola, R.; Garbassi, F.; Humphrey, P.; Johnson, D. *J. Colloid Interf. Sci.* **1990**, *137*, 11−24.
(24) Dong, C.; Gu, Y.; Zhong, M.; Li, L.; Sezer, K.; Ma, M.; Liu, W. *J. Mater. Process. Tech.* **2011**, *211*, 1234−1240.
(25) Kietzig, A. M.; Hatzikiriakos, S. G.; Englezos, P. *Langmuir* **2009**, *25*, 4821−4827.
(26) Kietzig, A. M.; Negar Mirvakili, M.; Kamal, S.; Englezos, P.; Hatzikiriakos, S. G. *J. Adhes. Sci. Technol.* **2011**, *25*, 2789−2809.
(27) Guo, Z.; Liang, J.; Fang, J.; Guo, B.; Liu, W. *Adv. Eng. Mater.* **2007**, *9*, 316−321.
(28) Qu, M.; Zhang, B.; Song, S.; Chen, L.; Zhang, J.; Cao, X. *Adv. Funct. Mater.* **2007**, *17*, 593−596.
(29) Tsujii, K.; Yamamoto, T.; Onda, T.; Shibuichi, S. *Angew. Chem. Int. Ed.* **1997**, *36*, 1011−1012.
(30) Wu, W.; Wang, X.; Wang, D.; Chen, M.; Zhou, F.; Liu, W.; Xue, Q. *Chem. Commun.* **2009**, 1043−1045.
(31) Guo, Z.; Zhou, F.; Hao, J.; Liu, W. *J. Am. Chem. Soc.* **2005**, *127*, 15670−15671.
(32) Saleema, N.; Sarkar, D. K.; Gallant, D.; Paynter, R. W.; Chen, X. G. *ACS Appl. Mater. Interfaces* **2011**, *3*, 4775−4781.
(33) Song, J.; Xu, W.; Lu, Y. *J. Mater. Sci.* **2011**, *47*, 162−168.
(34) Jafari, R.; Farzaneh, M. *Appl. Phys. A-Mater.* **2011**, *102*, 195−199.
(35) Men, X.; Zhang, Z.; Yang, J.; Zhu, X.; Wang, K.; Jiang, W. *New J. Chem.* **2011**, *35*, 881−886.
(36) Ho, K.; Newman, S. *Int. J. Mach. Tools Manuf.* **2003**, *43*, 1287−1300.
(37) Chung, D. K.; Shin, H. S.; Park, M. S.; Kim, B. H.; Chu, C. N. *Int. J. Precis. Eng. Manuf.* **2011**, *12*, 371−380.
(38) Chung, D. K.; Kim, B. H.; Chu, C. N. *J. Micromech. Microeng.* **2007**, *17*, 867−874.
(39) Kunieda, M.; Lauwers, B.; Rajurkar, K.; Schumacher, B. *CIRP Ann.-Manuf. Technol.* **2005**, *54*, 64−87.
(40) Bleys, P.; Kruth, J. P.; Lauwers, B.; Schacht, B.; Balasubramanian, V.; Froyen, L.; Van Humbeeck, J. *Adv. Eng. Mater.* **2006**, *8*, 15−25.
(41) Mohd Abbas, N.; Solomon, D. G.; Fuad Bahari, M. *Int. J. Mach. Tools Manuf.* **2007**, *47*, 1214−1228.
(42) Starke, E.; Staley, J. *Prog. Aerosp. Sci.* **1996**, *32*, 131−172.
(43) Owens, D. K.; Wendt, R. C. *J. Appl. Polym. Sci.* **1969**, *13*, 1741−1747.
(44) Nanz, G.; Camilletti, L. E. *IEEE Trans. Semicond. Met.* **1995**, *8*, 382−389.
(45) Chung, D. K.; Shin, H. S.; Kim, B. H.; Chu, C. N. *Int. J. Precis. Eng. Manuf.* **2011**, *12*, 1125−1128.
(46) Chen, Z.; Guo, Y.; Fang, S. *Surf. Interface Anal.* **2010**, *42*, 1−6.
(47) Suh, K. Y.; Park, M. C.; Kim, P. *Adv. Funct. Mater.* **2009**, *19*, 2699−2712.